Chie-Chieh Lin[1]
Fu-Hsiang Ko[1]
Chun-Chi Chen[1]
Yuh-Shyong Yang[2]
Feng-Chi Chang[1]
Chung-Shu Wu[1]

[1]Department of Materials Science and Engineering, Institute of Nanotechnology, National Chiao Tung University, Hsinchu, Taiwan
[2]Institute of Biological Science and Technology, National Chiao Tung University, Hsinchu, Taiwan

Received February 27, 2009
Revised May 31, 2009
Accepted June 5, 2009

Research Article

Miniaturized metal semiconductor metal photocurrent system for biomolecular sensing *via* chemiluminescence

A miniaturized metal semiconductor metal photodetector was developed as the core detector for chemiluminescence biosensor. The biosensor utilized the semiconductor manufacturing to fabricate the 83 interdigitated patterns of 250-nm metal line and 278-nm space in 100 μm × 100 μm active region. The established real-time detector was operated at 0.4 V to ensure the maximal signal to background ratio of 3600 under illumination intensity of 1.46 mW/cm^2. A chemiluminescence in the miniaturized chamber was successfully proposed to determine the model protein concentration in real-time analysis. Before the emission of light from the catalytic reaction of substrate, the model protein of streptavidin bound to horseradish peroxidase was successfully immobilized onto the sensor surface through the high-affinity conjugate with biotin. The detection limit of 4.76 nM for streptavidin analysis was obtained under the calibration curve of linear range over 5–100 nM with correlation coefficient of 0.9999.

Keywords:
Biosensor / Chemiluminescence / Metal semiconductor metal photodetector / Model protein analysis
DOI 10.1002/elps.200900120

1 Introduction

Over the past two decades, immense progress has been made in microelectronics and biotechnology for advanced biosensor development. There is a general trend for the new generation of biosensor toward real-time and more decentralized diagnostics [1–5]. Thus, the development of a sensitive, reliable, fast response, low-cost, and easy-to-set up biosensor system has become the most challenging issue in the healthcare industry [6–12]. The semiconductor manufacturing provides a stable and reliable platform for mass production of any designed chips of interest. In general, however, integrated semiconductor devices with sophisticated chemiluminescence analysis are still not commonplace.

Optical biosensors possess high sensitivity, ease of operation, high accuracy, and wide detection capacity [13–25]. In particular, luminescence-based optical biosensors exhibit some advantages, *i.e.* a low-detection limit, insensitivity to electrical disturbance, and a wide linear working range over conventional electrochemical biosensors [26, 27]. Most luminescent sensors are developed based on optical fiber technology; the light signals are transmitted from the luminescent reagents to the PMT by a waveguide medium. This design requires an expensive setup, *i.e.* a PMT and associated equipments, and limits the applications of the fiber-optic biosensors to the development of simple portable devices for real-time diagnosis. The PMT has characters of bulk appearance, large cost, and high power consumption, which limit its portable application to personalized or field-used instruments. To overcome the PMT limitation, Spohn *et al.* attempted to fabricate a miniaturized optical biosensor by replacing the PMT with a photodiode to detect the luminescence directly [15]. Vos *et al.* [1] also proposed optical microring resonator to monitor the wavelength shift of evanescent light. This silicon-on-insulator biochip can be integrated into a microflow system for lab-on-a-chip applications.

As to the issue of a portable biosensor system, the chemiluminescence and electrochemical detection mechanisms are the two possible candidates. The electrochemical sensing approach for biosensor has recently gained interests but not as well developed as optical techniques. Levine *et al.* developed active complementary metal oxide semiconductor (CMOS) sensor array for electrochemical biomolecule detection [6, 7]. The electrochemical molecule detection relies on detecting the real-time signal change owing to hybridization at the interface between a metal working electrode and a conductive target analyte solution. However, the complexity of electrochemical biomolecule analysis including both system setup and cost are complex and expensive in comparison with optical system. Daniel *et al.* proposed a whole-cell bioluminescent biosensor based on silicon

Correspondence: Dr. Fu-Hsiang Ko, Institute of Nanotechnology, National Chiao Tung University, Hsinchu 300, Taiwan
E-mail: fhko@mail.nctu.edu.tw
Fax: +886-357-44689

Abbreviations: APTES, 3-aminopropyltriethoxysilane; **CMOS,** complementary metal oxide semiconductor; **E-beam,** electron beam; **HRP,** horseradish peroxidase; **MSM-PD,** metal semiconductor metal photodetector; **NHS-Biotin,** (+)-biotin *N*-hydroxysuccinimide ester

photodiode [13]. This design demonstrates various advantages such as high sensitivity, wide dynamic range, and relatively inexpensive instruments. We recently [22–24] developed the miniaturized optical biosensors that were fabricated by integrating a CMOS-based photodiode, sol–gel technology, and coupled redox enzyme pair. A highly transparent organic–inorganic hybrid material was adopted to immobilize enzymes onto the CMOS photodiode to fabricate the optical biosensor. The biosensor was demonstrated to be very efficient on detecting the enzyme-catalyzed luminescence during real-time operation. However, the detection limit of micromolar (μM) level was not satisfactory. In addition, the development of the CMOS optical biosensor was very complicated. A couple of semiconductor manufacturing, such as impurity doping, multiple-patterning processes, and thin-film depositions, was required to fabricate the CMOS device. To overcome the drawbacks of CMOS-based biosensor, an alternating metal semiconductor metal photodetector (MSM-PD) is proposed here due to the issue of easy fabrication, better sensitivity, and low power consumption.

The MSM-PD devices are mainly applied in optical communication field [28–31]. Various types of light absorption materials in MSM-PD devices cover the wavelength ranging from ultraviolet to infrared, *i.e.* high frequency and low frequency. In general, wide bandgap materials are utilized for ultraviolet wavelength (high frequency) range and low bandgap materials for infrared wavelength (low frequency). Employed with further doping techniques in the absorption layer, the bandgap can be modulated for specific wavelength of interest [32]. The MSM-PD devices exhibit the property of low cost, less manufacturing time, great sensitivity, low power consumption, and fast-switching capability and thus demonstrate the capability to replace CMOS device as optical biosensor for portable system consideration. To the best of our knowledge, so far no MSM-PD device with miniaturized chamber has been proposed for protein-sensing application.

In this study, a novel miniaturized MSM-PD biosensor is developed by integrating the silicon chip with interdigitated structure, PDMS chamber, and chemiluminescence method. The MSM-PD-based biosensor demonstrates high detection capability, fast response, and a small amount of sample volume. The chemical immobilization procedure for model protein of streptavidin is used to verify the effectiveness of MSM-PD devices. The strategy of utilizing the luminescent molecule and enzyme system to benefit the model protein analysis is also developed. A method of luminescent signal acquisition is proposed for the real-time quantification of the model protein.

2 Materials and methods

2.1 Device-fabrication process

The instruments in Fig. 1 were constructed from the MSM-PD device, PDMS chamber, HP 4156 semiconductor analyzer (Agilent, USA), a home-made black (electromagnetic shielding) box, and a common personal computer. The SEM image was recorded using a JEOL JSM-6700F electron microscope (Tokyo, Japan) operated at 20 kV.

The materials and processes of the MSM-PD device illustrated in Fig. 2A used standard semiconductor manufacturing. Single-crystalline N^+-type $<100>$ silicon wafers with resistance 2–7 Ω cm were used in the experiment. First, 350 nm of silicon dioxide was deposited by low-pressure furnace tube to serve as pad oxide. Then, the substrate was coated with electron beam (E-beam) positive resist (ZEP-520, Zeon Chemicals, Tokyo, Japan) and followed by E-beam lithographic tool (Leica Weprint Model-200 stepper, Jena, Germany) with 40 keV beam energy and 20 nm beam size. After pattern exposure for defining the active region, the resist film was developed by immersing in 2.38% tetramethyl ammonium hydroxide solution to remove the resist from the active region. The silicon dioxide film in active region was then removed by reactive-ion-etching machine. The dimension of active region was 100 μm^2. Once the active region was defined, E-beam lithography was employed to fabricate the pattern of interdigitated resist lines. The 10 nm of chromium and 20 nm of gold were sequentially deposited onto the patterned substrate, followed by the lift-off method to reveal the metal lines. Finally, the 90-nm thickness of silicon dioxide was deposited by plasma-enhanced chemical vapor deposition. Before the PDMS chamber package, the MSM-PD device was cleaned in 120°C piranha solution (H_2SO_4:H_2O_2 = 7:3) for 1 h duration. The Sylgard 184 agent (Dow Corning) was mixed at a ratio of 10:1 (rubber base:cure) to form the PDMS solution. The solution was degassed within a vacuum chamber and then poured onto the designed aluminum template and cured at 70°C for 1 h to provide the PDMS mold. The inner diameter of PDMS chamber in Fig. 1 was 5 mm and the height was 1 cm. PDMS reaction chamber was packaged with MSM-PD device through oxygen plasma (Harrick Plasma PDC-32G, NY, USA) under 2 torr oxygen pressure for 10 min. The PDMS was then immersed in deionized water to form the

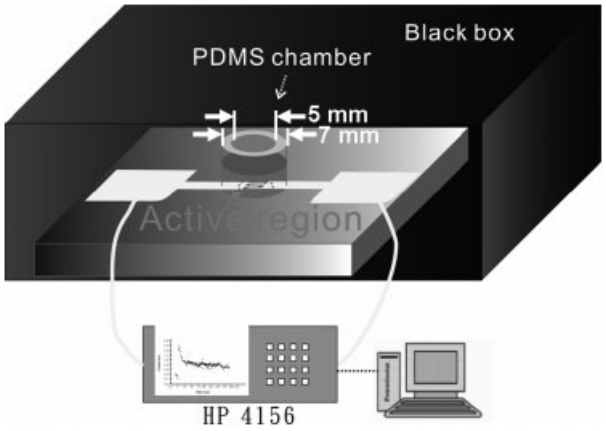

Figure 1. Schematic diagram of developed metal semiconductor metal-based photodetector system.

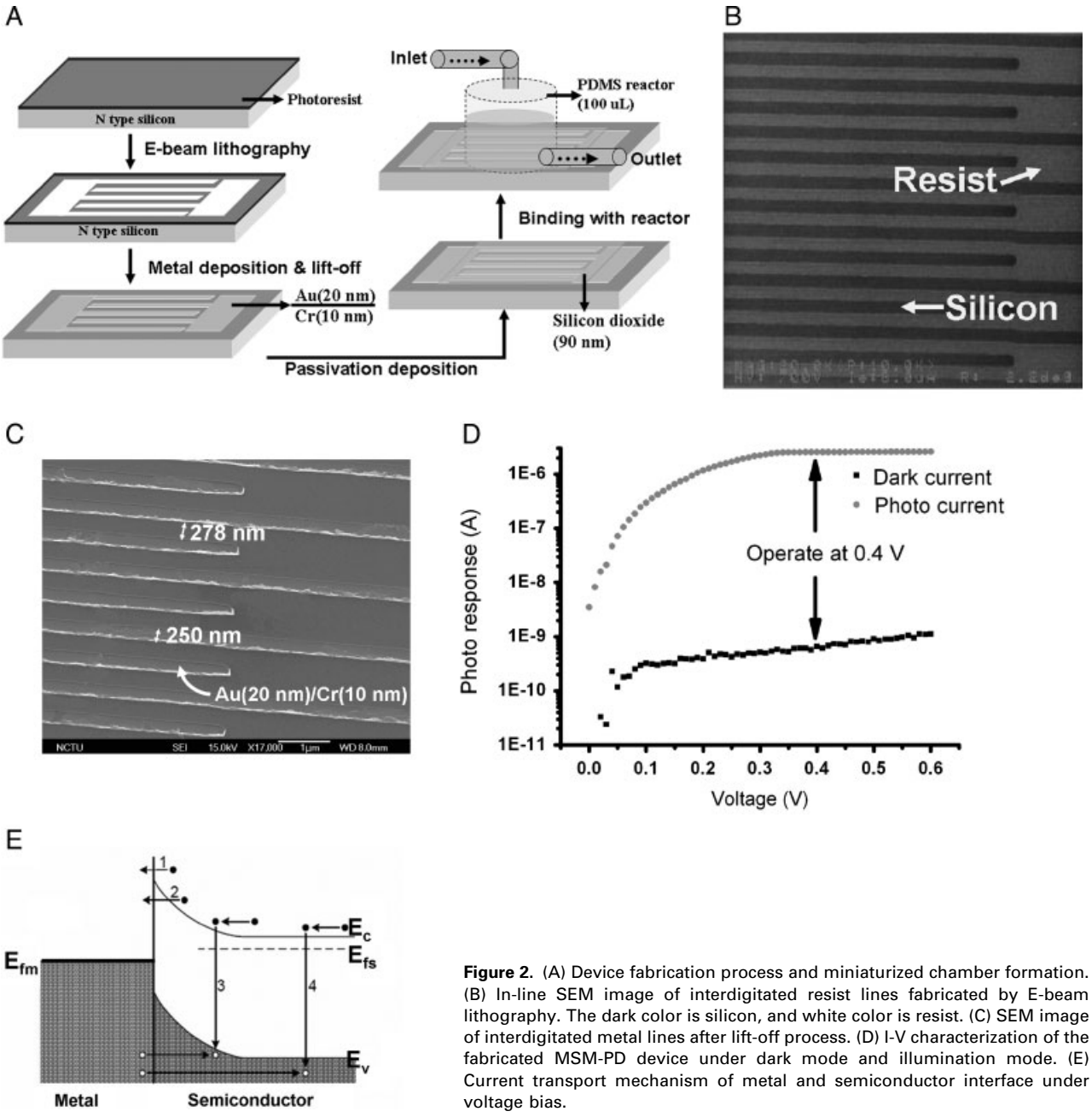

Figure 2. (A) Device fabrication process and miniaturized chamber formation. (B) In-line SEM image of interdigitated resist lines fabricated by E-beam lithography. The dark color is silicon, and white color is resist. (C) SEM image of interdigitated metal lines after lift-off process. (D) I-V characterization of the fabricated MSM-PD device under dark mode and illumination mode. (E) Current transport mechanism of metal and semiconductor interface under voltage bias.

–OH function group [33, 34]. Finally, the sensor with attachment of PDMS chamber on MSM-PD device was annealed at 90°C for 15 min.

2.2 Immobilization of streptavidin–HRP process

The (+)-biotin *N*-hydroxysuccinimide ester (NHS-Biotin) 98% was purchased from Sigma (St. Louis, MO, USA). Streptavidin, luminol, horseradish peroxidase (HRP), and chemiluminescent peroxidase substrate were also obtained from Sigma. DMSO was available from Fisher (Springfield, NJ, USA). 3-aminopropyltriethoxysilane (APTES, 98%) was available from ICN Biochemicals (Aurora, OH, USA). H_2O_2 and H_2SO_4 were purchased from Merck (Darmstadt, Germany). Milli-Q water was obtained from Milli-Q purification water system (Millipore, Bedford, MA, USA). PBS (10 mM) was prepared by dissolving 8 g NaCl, 0.2 g of KCl, 1.43 g of $Na_2HPO_4 \cdot 2H_2O$, and 0.343 g of K_2HPO_4 in 1 L of water and was adjusted to pH 7.4 by HCl.

The streptavidin was bound with HRP by the following procedure. HRP was conjugated to streptavidin according to a modification of the periodate method by reductive amination [35, 36]. The reaction solution was prepared by mixing 10 mL of 10 mg/mL HRP solution (10 mM sodium phosphate, 150 mM NaCl; pH 7.2) and sodium periodate

solution (88 mM, 1 mL) for 20 min in the dark at room temperature. The color of the solution gradually changed from brownish to green. Then, the oxidized enzyme solution was purified by gel filtration using a column of Sephadex G-25. Next, the periodate-oxidized HRP solution (10 mg/mL, 6.6 mL) was added to a solution containing 10 mg of streptavidin in 1 mL of 200 mM sodium bicarbonate (pH 9.6) at room temperature for 2 h to form the initial Schiff base interactions. After mixing the conjugation solution, sodium cyanoborohydride was added to streptavidin–HRP mixed complex solution (10 μL of 5 M sodium cyanoborohydride *per* 1 mL of streptavidin–HRP complex solution) and the mixture incubated for 30 min at room temperature. Then, approximately 50 μL of 1 M ethanolamine solution (pH 9.6) was mixed with 1 mL of streptavidin–HRP reaction solution for blocking unreacted aldehyde sites for 30 min. Finally, streptavidin–HRP complex was purified through gel filtration using Sephadex G-25 (10 mM sodium phosphate, 150 mM NaCl; pH 7; at a concentration of 10 mg/mL).

The biosensor was immersed in 10% APTES dried toluene solution for 30 min at 25°C and then washed with toluene for several times. The sensor is dried in a 100°C oven for 15 min. The 10 mM NHS-Biotin in DMSO solution was spiked into the sensor chamber to react with the APTES-modified device for 6 h. The unreacted NHS-biotin was removed by water and 1% tween-20 in PBS solution. In addition, BSA was used to block the nonspecific binding. Finally, the streptavidin–HRP solution was eluted into the chamber and washed with PBS solution several times.

3. Results and discussion

3.1 Design and integration of the MSM-PD biosensor

The designed biosensor in Fig. 1 is composed of three parts, *i.e.* MSM silicon chip with PDMS cover, current-voltage parameter extraction tool, and probe station in a black box, which serves as the background light shielding and external electromagnetic field isolation. In the first part, the PDMS-minimized chamber was bound to the MSM-PD device directly. The package of PDMS material has been mentioned earlier. The chamber covered all the active region of the MSM-PD, and it could successfully avoid short circuit problem in the liquid state during the immobilization process. The active region of the MSM-PD device was 100 μm × 100 μm. In the active region, two metal pads are designed on either side and each metal pad connects 83 metal lines. These metal lines are interdigitated between two pads, and this design is beneficial for collection of photo-generated majority carrier current. The metal line width and space was 250 and 278 nm, respectively. The inner diameter of minimized PDMS chamber was 5 mm, while the outer diameter of this chamber was 7 mm. A flexible plug is used to seal the top region of chamber and the chamber volume is obtained as nearly 100 μL in Figs. 1 and 2A. It should be noted that the distance between the two metal pads was 8 mm. Before on-chip biosensing, the probe of HP 4156 semiconductor analyzer is wired onto the metal pad of MSM-PD device. The personal computer is connected to the system for applied voltage and current recording. The total development system is used for the real-time biomolecule analysis.

The sensitivity of luminescent biosensor is strongly depended on the distance (d) between luminescent molecule and MSM detector. The Inverse Square Law mentions that the illuminance (E, light intensity *per* unit area of a target surface) varies in inverse proportion to the square of the distance ($E = I/d^2$) [37]. Previous publications have proposed the CMOS-type biosensors and the respective passivation layers of silicon dioxide are 2 mm and 5 μm [23, 24]. The sensitivity for 5-μm thinner passivation layer is five orders of magnitude better than the 2-mm thicker passivation layer. This observation clearly suggests the critical effect of thickness of passivation layer on luminescent biosensing. To achieve higher sensitivity for luminescent biosensor, the design and fabrication of novel biosensor under ultimate thinner passivation layer is the premier challenge. We design the MSM-PD biosensor in relation to above criteria with 90-nm passivation layer of silicon dioxide between immobilized luminescent molecule and detector. The designed thickness of passivation layer of MSM-PD device is about 1/56 times thinner than the 5-μm passivation layer of the CMOS sensor. Hence, the photo-response signal of our MSM-PD device at fixed light intensity is at least three orders of magnitude stronger than the state-of-the-art CMOS sensor. The higher response signal is beneficial for the analytical sensitivity and reliability.

3.2 Device fabrication, characterization, and physics for the MSM photodetector

The semiconductor manufacturing is the most popular and available technique due to large-volume and low-cost merits. However, the fabrication of densely and narrowly interdigitated metal lines on semiconductor is still challenged during the device fabrication process. To achieve the interdigitated MSM-PD device, we fabricate the 250-nm metal line and 278-nm space by using the E-beam lithography. Figure 2B shows the interdigitated E-beam resist. In the interdigitated region, the white line represents the resist width of 278 nm, which will be lifted off on metal deposition. On the contrary, the dark region in Fig. 2B will be filled with 250 nm metal line after metal deposition and liftoff. We pay more attention to find the best condition for the lift-off process. Initially, we use the lift-off process of (i) immersing the metal-deposited sample in SPM (mixture solution of sulfuric acid and hydrogen peroxide (volume ratio of 7:3)) solution for 10 min and then cleaning the sample with water and (ii) sonication in water for 3 s and then nitrogen purge to dryness. However, the device yield is very poor. The final satisfactory condition is: (i) immersing

the sample in the *N*-methyl-2-pyrrolidone solution for 4 days; (ii) before immersion, in SPM solution for 10 min and cleaning the sample with water; and (iii) sonication in water for 3 s and then nitrogen purge to dryness. Figure 2C illustrates the SEM image for the interdigitated metal line after lift-off process. The pattern morphology verifies the successful fabrication of interdigitated pattern. Finally, the 90-nm thickness of silicon dioxide film as passivation layer is deposited to form the MSM-PD device.

To ensure the performance of the MSM-PD device, the intended halogen lamp illumination with 1.46 mW/cm^2 power density is utilized. Figure 2D demonstrates the performance of MSM-PD device from 0 to 0.6 V under dark and illumination modes. Both of the photo response curves abruptly increase with applied voltage from 0 to 0.1 V. This observation is attributed to the overcoming of Schottky barrier from initial bias for both modes. However, the photo-generated carriers in the depletion region of the silicon layer are not totally collected. The response curves for illumination mode gradually reach saturation ranging from 0.1 to 0.35 V, and the larger bias collects more carriers. At applied voltage higher than 0.35 V, the device reaches its saturation zone and the photo-generated carriers are totally collected. This observation means the arrival of equilibrium state between the photo-generated carrier rate and recombination rate. The response current (I) is consistent with the prediction of metal–semiconductor junction, *i.e.* $I\alpha(e^{qV/kT}-1)$ [38]; where q is the electronic charge, V the applied voltage, k the Boltzmann constant, and T the absolute temperature. Interestingly, the MSM-PD device demonstrates the superior sensitivity and stability at 0.4 V. When the applied voltage is higher than 0.4 V, photocurrent under illumination mode remains saturated but the dark current still increased. If applied voltage is less than 0.4 V, the signal will be relatively unstable due to the closeness with saturation point of 0.35 V. The ratio of response current under illumination mode (1.46 mW/cm^2) and dark mode is estimated to be about 3600 at 0.4 V.

Figure 2E explains the carrier transport mechanism of metal–semiconductor interface under voltage bias. When metal is in contact with semiconductor, the Schottky barrier will be formed in the interface. There exist four possible carrier transport pathways: (i) emission of electrons from the semiconductor over the top of the potential barrier into the metal, (ii) quantum mechanical tunneling of electrons through the barrier, (iii) recombination in the depletion region, and (iv) recombination in the neutral region. The observation of photo-generated current in Fig. 2D is attributed to the above mechanisms.

3.3 Chemiluminescence mechanism and molecular surface immobilization for the analysis of model protein

We have successfully developed a very sensitive and stable MSM-PD device, and this device will be applied to the analysis of model protein of streptavidin. However, the streptavidin does not emit any light of interest. A miniaturized MSM-PD system in combination with a luminol-H_2O_2-HRP chemiluminescence is proposed for the analysis of streptavidin. In Fig. 3, the streptavidin has previously bonded with HRP, and streptavidin–HRP immobilized MSM-PD surface is designed to catalyze the luminol-H_2O_2 substrate to produce 3-aminophthalic acid in an excited state. As the excited state relaxes to the ground state, the excess energy is liberated as a 450 nm wavelength, visible as blue light. Subsequently, the underlying MSM-PD device detects the chemiluminescence for the real-time analysis of streptavidin.

How to bind the streptavidin–HRP onto the MSM-PD device surface? In Fig. 4, the APTES is first assembled onto SiO_2 surface of 90-nm thickness through covalent bonding. We use the 1.46 mW/cm^2 halogen lamp to check the effectiveness of MSM-PD device after APTES immobilization. In the right spectrum of Fig. 4A, the lamp is switched on at 8.59 s and off at 28.31 s. The corresponding photo response explains that the MSM-PD device is workable. Next, the biotin is reacted with the APTES. The corresponding photo response in Fig. 4B also verifies the effectiveness of the device. Once the biotin is successfully attached, the streptavidin–HRP is conjugated through the specific and strong affinity between biotin and streptavidin. In Fig. 4C, the MSM-PD device is still effective after

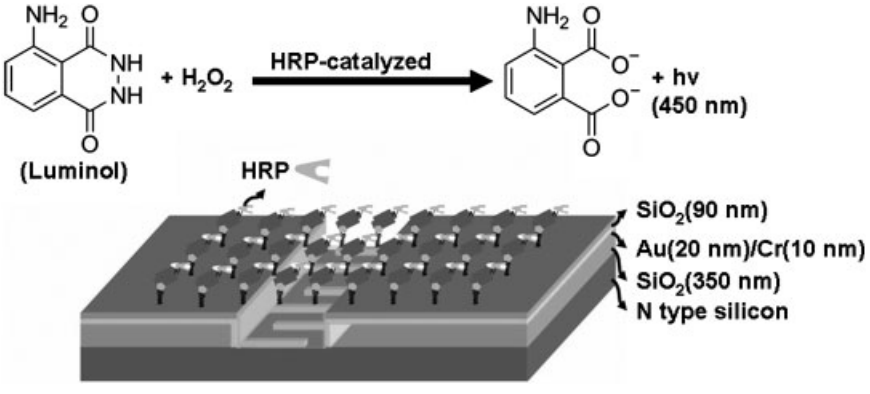

Figure 3. Chemical reaction of substrate of luminol and H_2O_2 under enzyme catalysis in the developed MSM-PD system.

streptavidin–HRP immobilization. Finally, the substrate of luminol and H_2O_2 is added into the PDMS chamber of biosensor to induce a chemiluminescence. Before this characterization, the halogen lamp is switched off. The HRP enzyme on the device surface can catalyze the luminescent reaction and produce blue light of interest. In Fig. 4D, the photocurrents at various times are recorded in real time for further analysis. The dark current represents the noise (background signal) of the system, and it is extremely important as it directly affects the precision and minimum

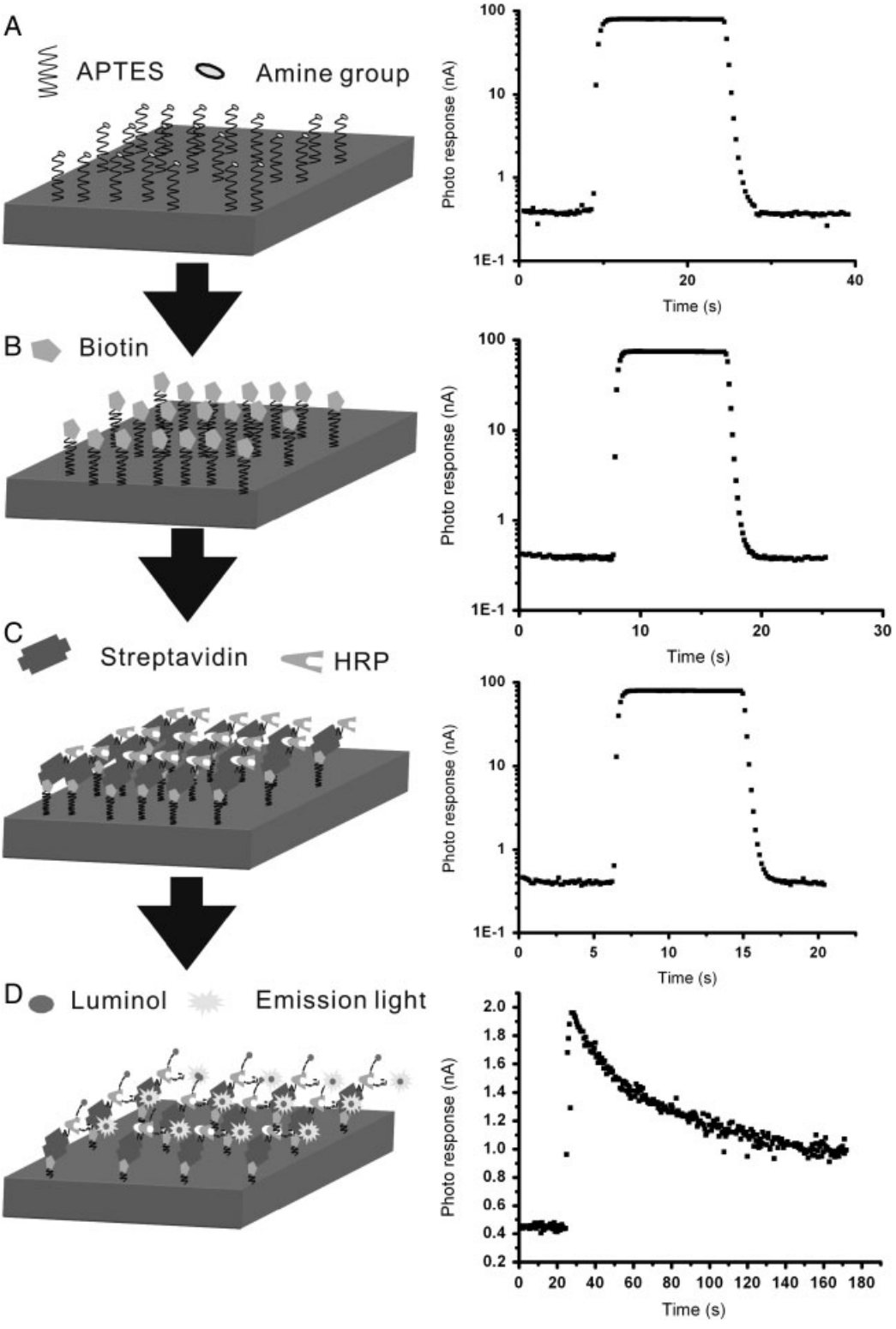

Figure 4. Detailed surface immobilization reaction and real-time photocurrent response for various molecules onto the developed MSM-PD chip. Real-time spectra are recorded under intended 1.46 mW/cm^2 halogen lamp for sensor with (A) APTES assembly, (B) biotin immobilization, and (C) streptavidin–HRP binding; dark environment for (D) substrate spiking.

detection limit of the system. Interestingly, the average dark currents are 0.43, 0.45, 0.44, and 0.44 nA for immobilization of APTES, biotin, streptavidin–HRP, and substrate, respectively. The similar dark current is attributed to the great shielding effect of proposed passivation layer of SiO_2. If the device's passivation fails, the liquid will contact the underlying metal line and lead to electrolysis. This phenomenon will provide an alternating current pathway and significantly increase the dark current. Additionally, the SiO_2 passivation layer can effectively avoid the effect of ion invasion from the PBS buffer. The ion invasion will increase the leakage current and seriously damage the MSM device. In short, the dark current is almost in the same value for various immobilization steps. This observation explains the better device stability and reliability, regardless of unadulterated or immobilized surfaces.

Before streptavidin analysis, the method for real-time signal acquisition needs to be clearly addressed. Figure 5 is an example of spectrum for the real sample by using our proposed MSM-PD biosensor in real-time detection. The sensor is operated in the black box, and the acquired signal (*i.e.* dark current) before adding substrate of luminol and H_2O_2 can be treated as the noise of the system. Once the fixed amount of substrate is spiked into the PDMS chamber, the surface-bound enzyme (*i.e.* HRP) immediately catalyzes substrate to produce chemiluminescence and the photo response current is abruptly increased. This observation suggests the HRP–luminol–H_2O_2 reaction is a flash type chemiluminescence reaction. At the peak, the maximal photon is emitted and induces the highest photo response current. After the peak, most of the substrate is consumed and the concentration is lowered. Therefore, the photo response current is gradually decayed. Hereafter, the analytical signal of our MSM-PD biosensor is defined as the difference of peak current and noise current.

To verify, the developed MSM-PD system can be used as an effective quantification biosensor; various concentrations (5–100 nM) of the model protein (*i.e.* streptavidin) are used to test the performance. The device is operated at 0.4 V and the scanning time interval is 0.5 ms. Figure 6A is the real-time spectrum for the blank sample. The blank sample

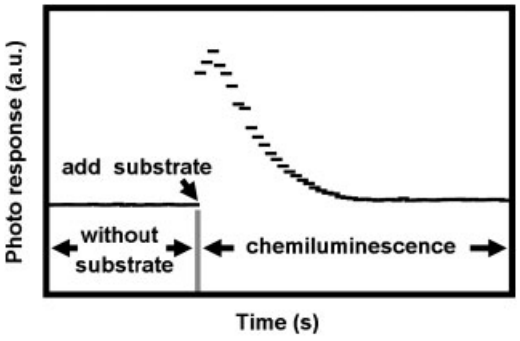

Figure 5. Typical real-time spectrum for the MSM-PD system under no substrate in the initial, substrate spiking, and chemiluminescence stage.

contains no streptavidin, and thus no enzyme is bound onto the biosensor's surface. There is no luminescent signal in the spectrum after the spiking of substrate. The average signal for blank sample in Fig. 6A is 0.45 nA, and the standard deviation is 0.03 nA. The relative standard deviation is about 6.7% for the blank sample. Figures 6B–E demonstrate the spectra for various proteins under the same substrate concentration of 100 μL. The analytical signals are 0.18, 0.59, 1.53, and 9.45 nA for the protein concentrations of 5, 10, 20, and 100 nM, respectively. As it can be seen from Figs. 6C–E, the half-height width is decreased with the enzyme concentration. What is the reason for the different shapes of these spectra? The reaction is based on first order; thus the reaction rate is proportional to the enzyme and substrate concentrations. Literature [39] has proposed the decisive parameters on the intensity of luminescent light in the following: $I(t) = (\alpha VA)K_f[\mathrm{E}][\mathrm{S}]$ where I is the light intensity, α the quantum yield, V the solution volume of substrate, A Avogadro's number, k_f the association rate constant for substrate and enzyme, [E] the enzyme concentration, t the time, and [S] the substrate concentration.

The higher concentration of streptavidin means the surface is bound with more enzymes. The more enzymes will consume the substrate more quickly and emit stronger luminescent light. Since the amount of substrate is consumed very quickly in the higher enzyme/streptavidin concentration, the analytical signal also quickly drops. This observation explains the reason for decrease in half-height width. Figure 6B behaves as an abnormal trend in comparison with Figs. 6C–E. The analytical signal is significantly affected by background signal due to the low concentration of enzyme/streptavidin. Furthermore, this concentration is near the detection limit of the MSM-PD biosensor.

The calibration curve in Fig. 6F is linear from 5 to 100 nM with correlation coefficient of 0.9999. The linear fitting for the calibration curve is $y = 0.0982 \times -0.377$, where y is the analytical signal (nA) and x the streptavidin concentration (nM). The detection limit of this biosensor is defined as streptavidin concentration that gives a signal intensity that is three times the standard deviation of the blank ($n = 7$). The method detection limit of the MSM-PD device is estimated as approximately 4.76 nM and better than the previous CMOS biosensors [22–24]. This result indicates that our miniaturized MSM-PD biosensor having a high sensitivity, better detection range, real-time capability, fast response, specific molecule biorecognition, and low fabrication cost can be used for future biomolecule detection.

4 Concluding remarks

In this study, a miniaturized optoelectronic-based chemiluminescence biosensor has been successfully developed. The optoelectronic biosensor demonstrates the capability for determining the enzyme-catalyzed luminescence in real-time

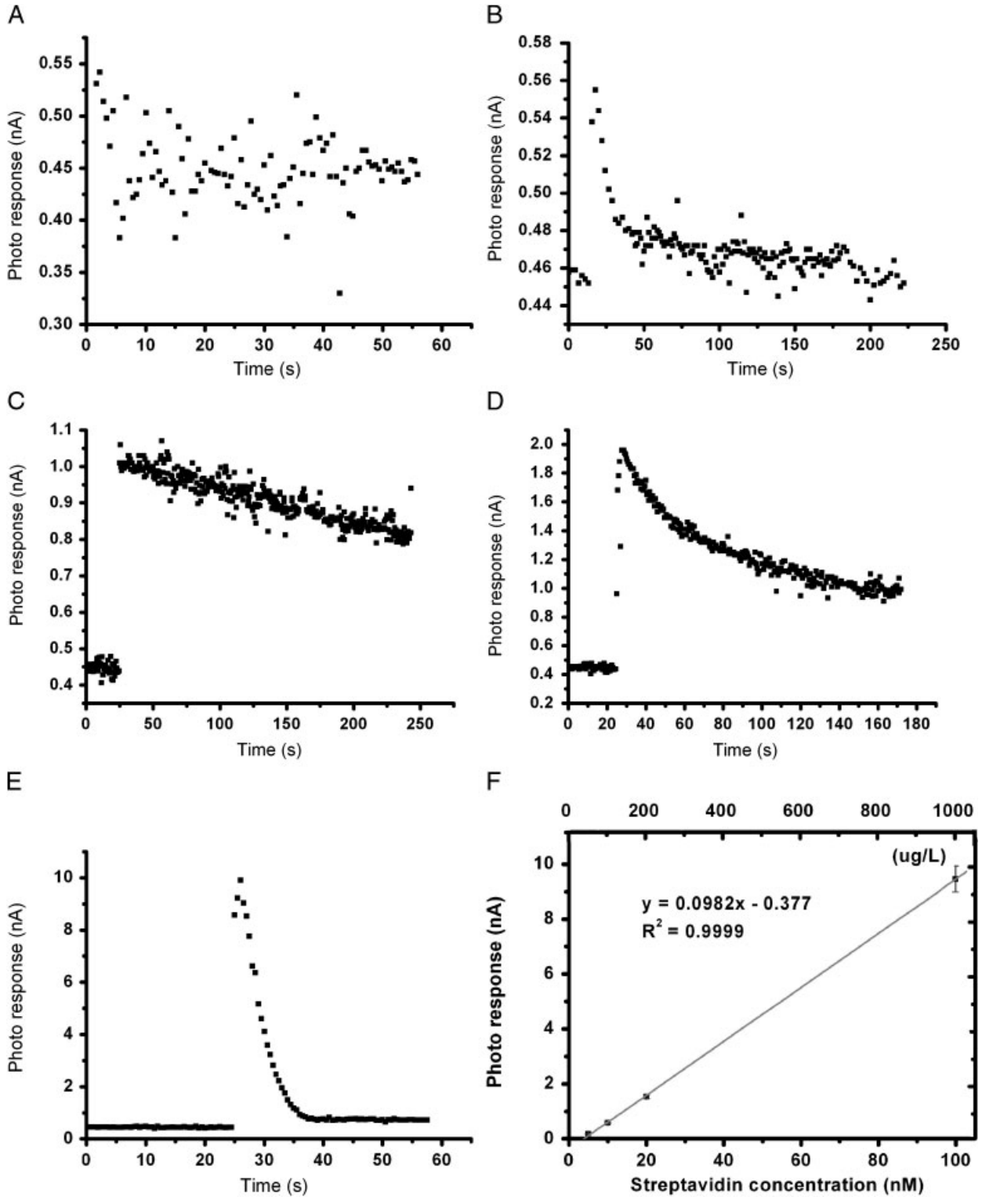

Figure 6. Real-time spectrum for (A) blank sample without model protein, (B) 5 nM streptavidin, (C) 10 nM streptavidin, (D) 20 nM streptavidin, and (E) 100 nM streptavidin. (F) Calibration graphs for various protein concentrations in the miniaturized MSM-PD biosensor. Each data presented as mean ± standard deviation from three replicates.

analysis. The thinner 90-nm passivation layer of silicon dioxide reduces the distance between the luminescent molecule and the MSM-interdigitated detector. Hence, the sensitivity of the miniaturized state-of-the-art MSM-PD biosensor is three orders of magnitude better than that of the CMOS biosensor. We successfully assemble enzyme with the model protein to conduct the chemiluminescence for substrate of luminol and hydrogen peroxide. The detection limit of 4.76 nM for streptavidin analysis is obtained under the calibration curve of linear range over 5–100 nM with correlation coefficient of 0.9999. The array-type biosensor featuring the rapid response, high sensitivity, and small sample volume may further apply in clinical diagnoses, food quality control, and environmental monitoring.

The research was financially supported by National Science Council, Taiwan (NSC 95-2113-M-009-032-MY3 and 97-2218-E-009 -002).

The authors have declared no conflict of interest.

5 References

[1] Vos, K. D., Girones, J., Popelka, S., Schacht, E., Baets, R., Bienstman, P., *Biosens. Bioelectron.* 2009, *24*, 2528–2533.

[2] Hofmann, O., Voirin, G., Niedermann, P., Manz, A., *Anal. Chem.* 2002, *74*, 5243–5250.

[3] Kwakye, S., Baeumner, A., *Anal. Bioanal. Chem.* 2003, *376*, 1062–1068.

[4] Askari, M., Alarie, J. P., Moreno-Bondi, M., VoDinh, T., *Biotechnol. Prog.* 2001, *17*, 543–552.

[5] Huang, X. Y., Ren, J. C., *Electrophoresis* 2005, *26*, 3595–3601.

[6] Levine, P. M., Gong, P., Levicky, R., Shepard, K. L., *IEEE J. Solid-State Circuits* 2008, *43*, 1859–1871.

[7] Levine, P. M., Gong, P., Levicky, R., Shepard, K. L., *Biosens. Bioelectron.* 2009, *24*, 1995–2001.

[8] Koga, H., Kyo, M., Kyo Kazue,K., Inamori, K., *Electrophoresis* 2006, *27*, 3676–3683

[9] Baeumner, A. J., Cohen, R. N., Miksic, V., Min, J., *Biosens. Bioelectron.* 2003, *18*, 405–413.

[10] Choi, S. H., Gu, M. B., *Biosens. Bioelectron.* 2002, *17*, 433–440.

[11] DeBusschere, B. D., Kovacs, G. T., *Biosens. Bioelectron.* 2001, *16*, 543–556.

[12] Blum, L. J., Gautier, S. M., Blum, L. J., Coulet, P. R., *Biosensor Principles and Applications*, Marcel Dekker, New York 1991, pp. 213–247.

[13] Daniel, R., Almog, R., Ron, A., Belkin, S., Diamand, Y. S., *Biosens. Bioelectron.* 2008, *24*, 882–887.

[14] Salama, O., Herrmann, S., Tziknovsky, A., Piura, B., Meirovich, M., Trakht, I., Reed, B. *et al.*, *Biosens. Bioelectron.* 2007, *22*, 1508–1516.

[15] Spohn, U., Preuschoff, F., Blankenstein, G., Janasek, D., Kula, M. R., Hacker, A., *Anal. Chim. Acta* 1995, *303*, 109–120.

[16] Chen, Z., Kaplan, D. L., Gao, H., Kumar, J., Marx, K. A., Tripathy, S. K., *Mater. Sci. Eng. C* 1996, *4*, 155–159.

[17] Marquette, C. A., Blum, L. J., *Anal.Chim. Acta* 1999, *381*, 1–6.

[18] Ruano, J. M., Benoit, V. V., Aitchison, J. S., Cooper, J. M., *Anal. Chem.* 2000, *72*, 1093–1097.

[19] Tsafack, V. C., Marquette, C. A., Pizzolato, F., Blum, L., *Biosens. Bioelectron* 2000, *15*, 125–133.

[20] Ivanov, Y. D., Kanaeva, I. P., Gnedenko, O. V., Pozdnev, V. F., Shumyantseva, V. V., Samenkova, N. F., Kuznetsova, G. P. *et al. J. Mol. Recognit.* 2001, *14*, 185–196.

[21] Askari, M. D., Miller, G. H., Vo-Dinh, T., *Cancer Detect. Prevent.* 2002, *26*, 331–342.

[22] Lu, U., Hu, B. C. P., Shih, Y. C., Yang, Y. S., Wu, C. Y., Yuan, C. J., Ker, M. D. *et al.*, *IEEE Sens.* 2003, *3*, 310–316.

[23] Huang, S. H., Shih, Y. C., Wu, C. Y., Yuan, C. J., Yang, Y. S., Li, Y. K., Wu, T. K., *Biosens. Bioelectron.* 2004, *19*, 1627–1633.

[24] Ho, W. J., Chen, J. S., Ker, M. D., Wu, T. K., Wu, C. Y., Yang, Y. S., Li, Y. K. e*t al.*, *Biosens. Bioelectron.* 2007, *22*, 3008–3013.

[25] Song, J. M., Culha, M., Kasili, P. M., Griffin, G. D., Vo-Dinh, T., *Biosens. Bioelectron.* 2005, *20*, 2203–2209.

[26] Zhang, J., Qi, H., Li, Y., Yang, J., Gao, Q, Zhang, C., *Anal. Chem.* 2008, *80*, 2888–2894.

[27] Borisov, S. M., Nuss, G., Klimant, I., *Anal. Chem.* 2008, *80*, 9435–9442.

[28] Kong, X. Z., Liu, C. X., Dong, W., Zhang, X. D., Tao, C., Shen, L., Zhou, J. R. e*t al. Appl. Phys. Lett.* 2009, *94*, 123502.

[29] Zhao, J. L., Tan, S. T., Iwan, S., Sun, X. W., Liu, W., Chua, S. J., *Appl. Phys. Lett.* 2009, *94*, 093506.

[30] Hwang, J. D., Hseih, K. H., *Microelectron. Eng.* 2008, *85*, 2266–2268.

[31] Zhu, S. Y., Lo, G. Q., Kwong, D. L., *IEEE Photonics Technol. Lett.* 2008, *20*, 1396–1398.

[32] Zhao, Y., Kita, K., Kyuno, K., Toriumi, A., *Appl. Phys. Lett.* 2009, *94*, 042901.

[33] Bhattacharya, S., Datta, A., Berg, J. M., Gangopadhyay, S., *J. Microelectromech. Syst.* 2005, *14*, 590–597.

[34] Sundararajan, N., Pio, M. S., Lee, L. P., Berlin, A. A., *J. Microelectromech. Syst.* 2004, *13*, 559–567.

[35] Ekong, T. A. N., Mclellan, K., Sesardic, D., *J. Immunol. Methods* 1995, *180*, 181–191.

[36] Hermanson, G. T., *Bioconjugate Techniques*, Academic Press, New York 1996.

[37] Halliday, D., *Fundamentals of Physics*, Wiley, New York 2004.

[38] Sze, S. M., *Semiconductor Devices, Physics and Technology*, Wiley, New York 1985.

[39] Salama, K., Eltoukhy, H., Hassibi, A., El Gamal, A., *Biosens. Bioelectron.* 2004, *19*, 1377–1386.

